

# A Broadband 3D Printed Fractal Tree Monopole Antenna

Kathryn Smith\* and Ryan Adams

**Abstract**—A broadband monopole antenna is presented, with a radiating body consisting of a fractal tree with three-dimensional conical branches. The effect on polarization and return loss of varying the number of branches, as well as the number of fractal iterations, is explored and presented. The best-case antenna, having five branches and three fractal iterations, was fabricated using a 3D-printed form covered in conductive spray paint. The return loss of this antenna was shown in both simulation and measurement to be better than  $-10$  dB from 1.22 GHz to 24.1 GHz, a bandwidth of more than 180%.

## 1. INTRODUCTION

The driving force behind broadband antenna development is the increasingly ubiquitous use of wireless communication. Thousands of everyday applications, from radio and cellular communication to bluetooth and wi-fi, require antennas to send and receive information. Every application has an assigned frequency spectrum, within which individual signals must find frequencies where noise from other nearby users will not obscure the signal. Multiple closely-spaced antennas often conflict with one another, as cross-talk between the various systems creates noise and changes the antenna radiation patterns. The ability to integrate multiple communication systems and consolidate to a single antenna resolves these issues, however, it requires that the single antenna be able to operate over a broad range of frequencies.

Fractal geometries are formed by scaled repetitions of a basic shape [1]. When applied to antennas, these geometries have been shown to support multiband and wideband performance, as different portions of the structure become dominantly active at different frequencies. This property is demonstrated clearly in [2], where a fourth-order Sierpinski fractal monopole antenna is reported to operate at multiple frequencies, with similar current patterns setting up in progressively smaller portions of the antenna as the frequency increased. It was also reported that at high frequencies the inactive portions acted as loading on the active portions, pulling their resonance to lower frequencies.

In [3], a two-dimensional fractal tree monopole antenna was presented. The fractal tree was formed of a simple repeating pattern in which every iteration expanded the existing branches by adding a split into two additional branches of the same size as the original. A curve in the ground plane was used to help match the radiating element to the microstrip feed line. Several versions of this antenna with various numbers of iterations were compared, to show the improvement offered by increasing complexity. This antenna had a height of 11.57 mm, and its measured  $S_{11}$  was reported to be below  $-10$  dB over a band from 2.1 GHz to 11.52 GHz.

A second two-dimensional fractal tree monopole antenna was presented in [4]. This antenna was also formed of splitting branches, but in this case each iteration consisted of smaller branches than the previous, based on a modified Pythagorean tree fractal. Again, a curved ground plane was used to match the radiating element to the microstrip feed line. This antenna had a height of 13.41 mm, and its measured  $S_{11}$  was reported to be below 10 dB from 2.6 GHz to 11.14 GHz. Other two-dimensional fractal tree antennas are presented in [5–7], among others.

---

*Received 5 March 2018, Accepted 18 July 2018, Scheduled 27 July 2018*

\* Corresponding author: Kathryn Smith (ksmit351@uncc.edu).

The authors are with the Department of Electrical and Computer Engineering at the University of North Carolina at Charlotte, 9201 University City Blvd, Charlotte, NC, USA.

As these examples demonstrate, two-dimensional fractal tree antennas are capable of maintaining excellent return loss over a wide band of frequencies. However, their radiation characteristics are poor, with high cross-polarization and asymmetric radiation in both the  $E$ -plane and the  $H$ -plane.

A collection of three-dimensional fractal tree dipole antennas consisting of very thin wires were presented in [8]. These antennas were shown to have multiple narrow bands of performance, tunable by changing the branch angles, number of rotational repetitions, and number of fractal iterations. Their radiation characteristics are much better than the two-dimensional antennas in [3, 4]. However, these antennas were explored only through simulation, because of the prohibitive complexity of fabricating such structures. In [9], a three-dimensional fractal tree formed through an electrochemical-deposition process is presented. This antenna was shown to offer multiband behavior, but its geometry is inherently random, because of the process by which it was formed. The frequencies at which it operates are thus unpredictable and do not conform to any design specifications.

The current work, building upon preliminary results from [10], presents a three-dimensional fractal tree monopole antenna with deterministic (rather than random) buildable dimensions, consisting of an iterated branching conical structure. This antenna is shown to have much better polarization behavior than the two-dimensional antennas of [3, 4], while increasing bandwidth to 180.7%. The effects of varying the number of branches per iteration and the number of iterations was explored through simulation in HFSS. Finally, the best of the simulated variations was fabricated with a 3D printer, and measured results are presented.

## 2. GEOMETRY OF CONICAL FRACTAL TREE MONOPOLE ANTENNA

The conical fractal monopole antenna presented in this paper consists of three iterations of progressively smaller alternating conical and interconnecting sections in a branching pattern, as shown in Fig. 1(a). This structure was initiated as a three-dimensional, conical expansion of the Pythagorean tree fractal presented in [4]. Each branch is formed of a cone with height  $h_{cn}$ , lower radius  $rl_n$ , and upper radius  $ru_n$ , and a circular tapering transition with height  $h_{rn}$ , lower radius  $ru_{n-1}$  and upper radius  $rl_n$ , where  $n$  is the iteration number. The vertical axis of each iteration is offset from the axis of the previous

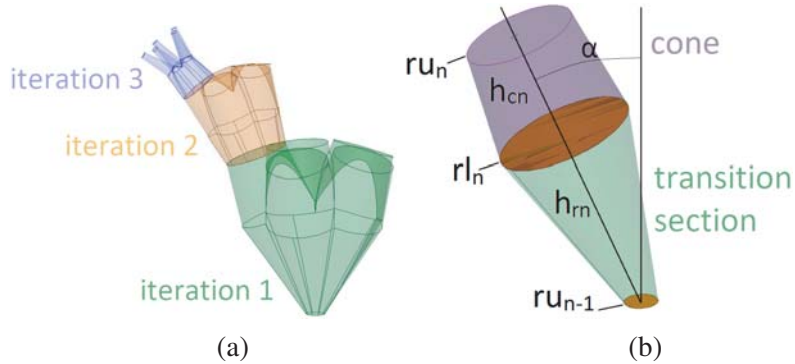


**Figure 1.** (a) Three fractal iterations of the conical fractal tree monopole antenna. (b) A detailed view of the geometry of the fractal tree initiator.

**Table 1.** Dimensions of conical fractal tree monopole antenna.

Iteration #	$rl$ (mm)	$ru$ (mm)	$h_c$ (mm)	$h_r$ (mm)
0	NA	1.475	NA	NA
1	7	4.9	10	17
2	4	3.02	7	7
3	1	0.5	5	5

iteration by  $\alpha = 20^\circ$ . Fig. 1(b) shows a single branch of the iterative shape. The cone is the upper half of the branch, and the transition section is the lower half. It should be noted that the transition section is formed as a connection between the two circles at its ends. The lower circle is normal to the axis of iteration  $n - 1$ , and the upper circle is normal to the axis of iteration  $n$ . Since the circles are not parallel, this section is not a cone. Each progressive iteration is built on the previous by using the upper tip of the  $n$ th cone as the lower circle of the  $(n + 1)$ th transition section. Each of these parameters was varied from the initial Pythagorean-tree based architecture in HFSS to obtain the optimal dimensions for each fractal iteration. The dimensions of the three-iteration conical fractal tree monopole antenna resulting from this optimization are given in Table 1.

An  $N$ -pronged structure is formed by duplicating each iteration around the axis of the previous iteration  $N$  times, at intervals of  $\frac{360^\circ}{N}$ . The antenna is matched to an RG-58C/U  $50 \Omega$  coaxial line using a hemisphere of an oblate spheroidal shaped ground, having a major axis of 25 mm and a minor axis of 15 mm. There is a gap between the ground and the fractal of 0.8 mm.

### 3. SIMULATION OF CONICAL FRACTAL TREE MONOPOLE ANTENNA

This section will present several variations on the conical fractal tree monopole antenna, and evaluate each with respect to return loss and radiation pattern. One of these antennas will be selected for

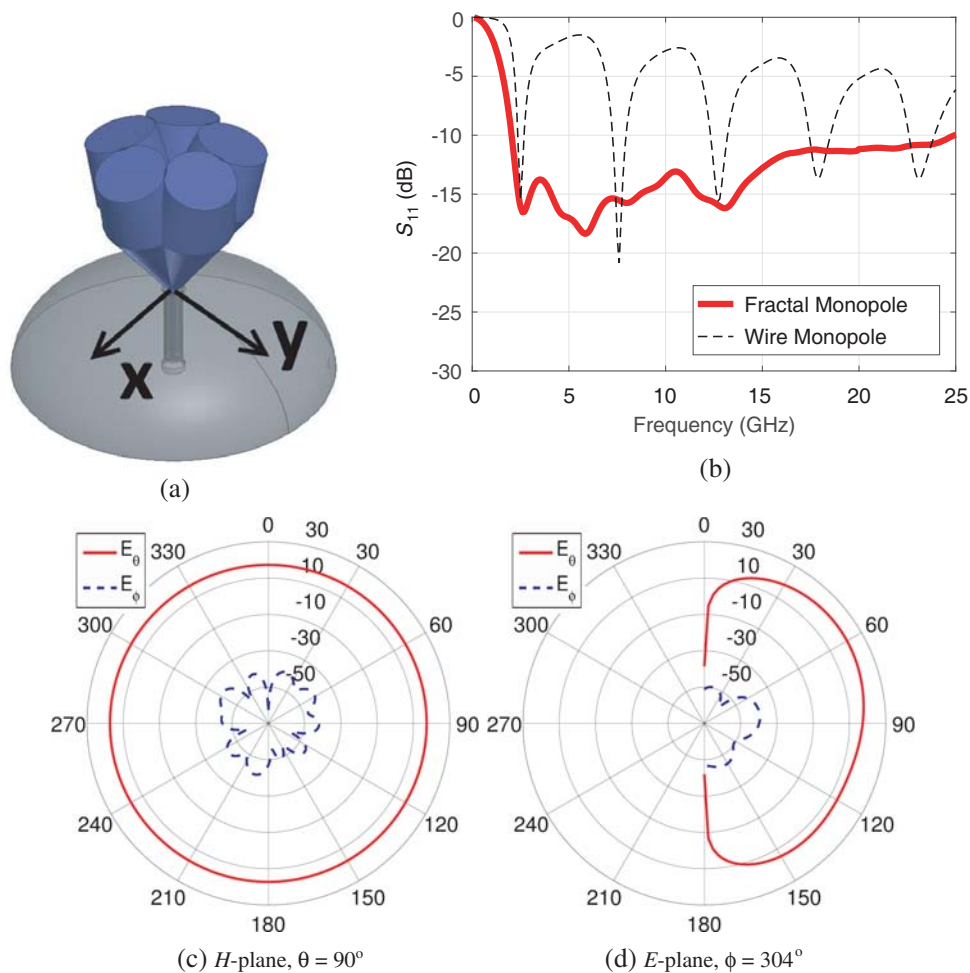


**Figure 2.** (a) A five-pronged, single-iteration fractal tree monopole antenna. (b) The corresponding return loss. (c) The corresponding broadside  $H$ -plane radiation pattern at 5.5 GHz. (d) The corresponding worst-case  $E$ -plane radiation pattern at 5.5 GHz.

fabrication and measurement in the succeeding section. Two major variants are explored — firstly, the number of fractal iterations, and secondly, the number of duplications around the  $z$ -axis, or “prongs”. Each of the antennas was simulated in a cylindrical air box with a diameter of 90 mm and a height of 95.8 mm. These dimensions were chosen so that the largest of the antennas was separated from the air box by at least  $\lambda/4 = 15$  mm at 5 GHz. There was also a mesh operation defined on the surface of the air box, which constrained the mesh length on that surface to  $\lambda/6 = 5$  mm at 10 GHz. These constraints were required to allow HFSS to perform a near to far field transformation valid from 5 GHz to 10 GHz. It was desirable to minimize the range of frequencies over which the far field simulation was valid, to speed simulation and prevent an unreasonable number of tetrahedra from being required to solve the problem. The consistent size of the air box allows meaningful comparison of the number of tetrahedra used for each simulation, which provides a rough measure of the complexity of the design.

The first antenna to be evaluated is a five-pronged fractal tree monopole antenna with a single fractal iteration, shown in Fig. 2(a). This antenna has an approximate height, not including the ground, of 28 mm, and an approximate radius, not including the ground, of 15 mm. The antenna was simulated in Ansys HFSS, using a mesh of 69,312 tetrahedra, and a convergence criteria of  $|\Delta S| < 0.01$  for two consecutive adaptive passes. The return loss for the antenna resulting from this simulation is shown in Fig. 2(b) in solid red. This antenna shows return loss less than  $-10$  dB from 2 GHz to 24.9 GHz,

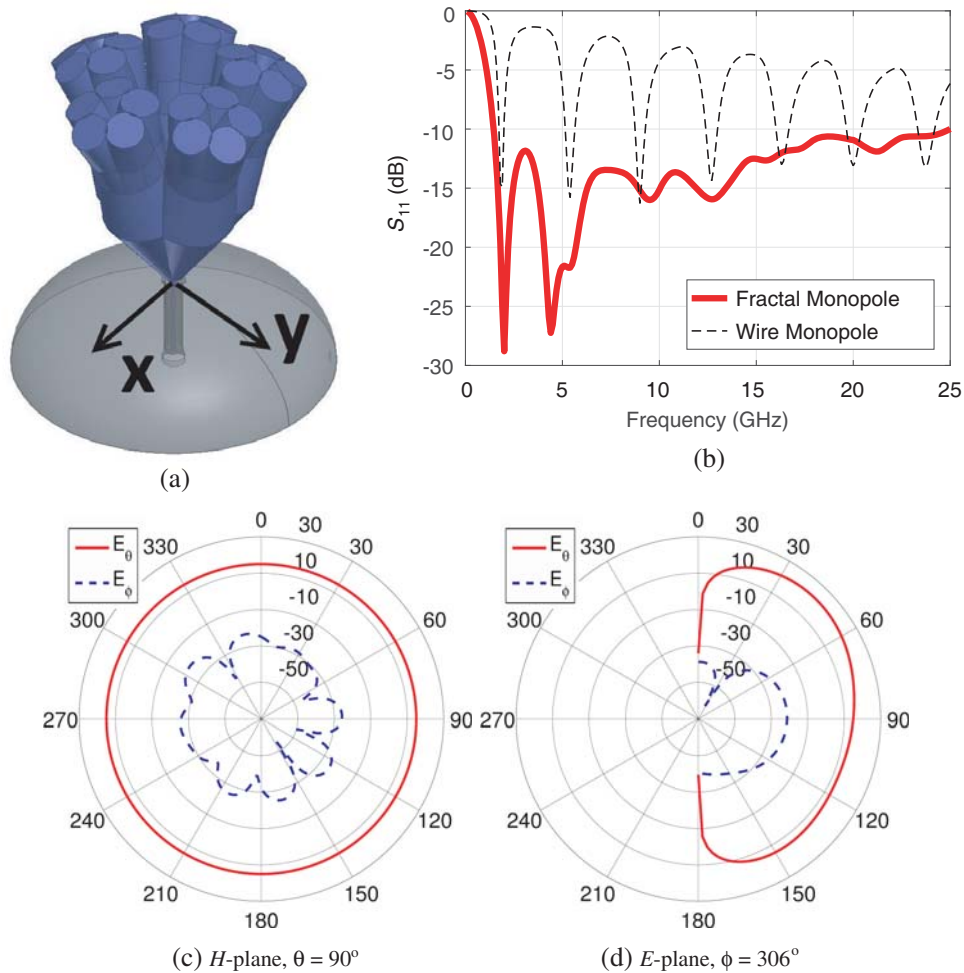


**Figure 3.** (a) A five-pronged, two-iteration fractal tree monopole antenna. (b) The corresponding return loss. (c) The corresponding broadside  $H$ -plane radiation pattern at 5.5 GHz. (d) The corresponding worst-case  $E$ -plane radiation pattern at 5.5 GHz.

corresponding to a bandwidth of 170.3%. Local minima may be observed in this plot at 2.6 GHz, 5.9 GHz, 8 GHz, and 13.1 GHz. For comparison, the return loss for a wire monopole antenna having the same length and semi-elliptical ground as the fractal antenna is also shown, in dashed black. The broadside  $H$ -plane radiation pattern for this single-iteration fractal tree monopole antenna at a representative frequency of 5.5 GHz is shown in Fig. 2(c). The worst-case cross polarization shown in this plot occurs at  $\phi = 304^\circ$ , where the cross-polarized power is 57 dB below the co-polarized power. The corresponding worst-case  $E$ -plane radiation pattern is shown in Fig. 2(d).

The second antenna is shown in Fig. 3(a). This is a five-pronged fractal tree monopole antenna with two fractal iterations. This antenna has an approximate height, not including the ground, of 40 mm, and an approximate radius, not including the ground, of 21 mm. The simulation converged using 90,057 tetrahedra, with  $|\Delta S| < 0.01$  for two consecutive passes. Fig. 3(b) shows the return loss of this antenna in dB, and Figs. 3(c) and 3(d) show its broadside  $H$ -plane and worst-case  $E$ -plane radiation patterns at 5.5 GHz. As shown, the five-pronged, two-iteration fractal antenna has return loss better than  $-10$  dB starting at approximately 1.43 GHz and continuing to 24.9 GHz. This corresponds to a bandwidth of 178.3%. Local minima may be observed in this plot at 2 GHz, 4.4 GHz, 5.4 GHz, 9.5 GHz, 12.7 GHz, 15.5 GHz, and 21.2 GHz. Like the single-iteration antenna, this antenna has a smooth, symmetric broadside radiation pattern, with very good polarization characteristics. The broadside cross-polarization of this antenna is better than 36 dB, with the worst-case broadside polarization occurring

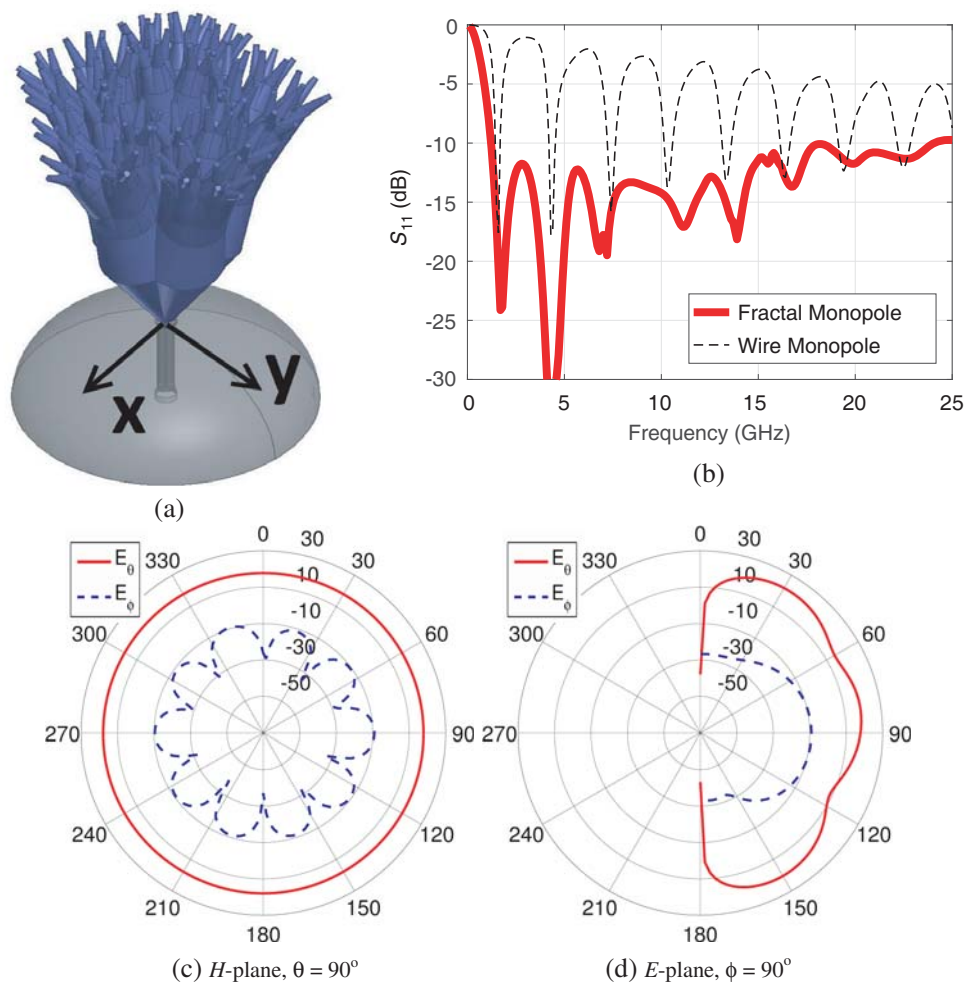


**Figure 4.** (a) A five-pronged, three-iteration fractal tree monopole antenna. (b) The corresponding return loss. (c) The corresponding broadside  $H$ -plane radiation pattern at 5.5 GHz. (d) The corresponding worst-case  $E$ -plane radiation pattern at 5.5 GHz.

at  $\phi = 306^\circ$ . The  $E$ -plane radiation maintains the smoothness with respect to  $\theta$  of the previous model.

A three-iteration model was simulated next. This antenna, shown in Fig. 4(a), has a height of approximately 51 mm, not including the ground, and a radius of approximately 27 mm. The simulation converged with 210,702 tetrahedra, after two consecutive passes with  $|\Delta S| < 0.01$ . This simulation results in the return loss shown in Fig. 4(b). Local minima may be observed in this plot at 1.7 GHz, 4.2 GHz, 6.8 GHz, 7.2 GHz, 11.1 GHz, 13.9 GHz, 15.5 GHz, 16.8 GHz, and 19.9 GHz. The radiation pattern and cross-polarization at 5.5 GHz is shown in Figs. 4(c) and 4(d).

These plots show that the five-pronged, three-iteration fractal tree monopole antenna exhibits return loss less than  $-10$  dB over the range 1.22 GHz–24.1 GHz, corresponding to a bandwidth of 180.7%. Its radiation pattern maintains symmetry with respect to  $\phi$ , but the smoothness of the  $E$ -plane pattern with respect to  $\theta$  is slightly degraded in comparison to the previous two models. At 5.5 GHz, the broadside cross-polarization of this antenna is better than 27 dB below the co-polarized power. The cross-polarization also notably has ten distinct lobes, with minima at  $\phi = 0^\circ$  and at  $36^\circ$  intervals all the way around, corresponding to both the prongs and the valleys of the radiating body of the antenna. This variation is a product of the fact that the fractal geometry results in a current distribution around the body of the antenna that is non-uniform with respect to  $\phi$ .

Because of the resolution limitations of the 3D printer used for fabrication, further increase of the number of iterations was not feasible.

Table 2 summarizes the results of these three simulations, for easy comparison. As shown, the bandwidth increases by 8% from the single-iteration model to the two-iteration model, but only increases by 2.4% from the two-iteration model to the three-iteration model. The cross-polarization degrades by 20.7 dB from the single-iteration model to the two-iteration model, and degrades by a further 9.3 dB from the two-iteration model to the three-iteration model. Assuming this trend holds, a fourth iteration would increase the bandwidth only marginally, while the cross-polarization would become significantly worse. Of the three models that were simulated, the three-iteration model has the highest bandwidth, while also maintaining good cross polarization.

**Table 2.** Summary of the simulation results for the one-iteration, two-iteration, and three-iteration five-pronged fractal tree monopole antenna models at 5.5 GHz.

# of Iterations	Height (mm)	Radius (mm)	Bandwidth (%)	Broadside Cross-pol (dB)	# of Tetrahedra
1	28	15	170.3	57.0	69,312
2	40	21	178.3	36.3	90,057
3	51	27	180.7	27.0	210,702

All three of the antennas simulated thus far were five-pronged antennas. The following discussion explores the effect of changing the number of prongs on the antenna. Three-pronged, four-pronged, and six-pronged fractal variations are presented. Each of these antennas has an overall height, not including the ground, of approximately 51 mm, and a maximum radius of 27 mm. They were each simulated in Ansys HFSS, using a convergence criteria of  $|\Delta S| < 0.01$  for two consecutive passes.

The three-pronged version of the fractal monopole antenna is shown in Fig. 5(a). The simulation of this antenna converged with 128,303 tetrahedra. The magnitude of  $S_{11}$  in dB resulting from this simulation is shown in Fig. 5 in solid red. Again,  $S_{11}$  for the case of the wire monopole antenna with corresponding length and ground is shown in dashed black for comparison. The return loss is below  $-10$  dB from approximately 1.26 GHz to 18 GHz, corresponding to a bandwidth of 173.0%. Local minima may be observed in this plot at 1.7 GHz, 4 GHz, 4.8 GHz, 6.8 GHz, 11.1 GHz, 13.5 GHz, 16.6 GHz, 20 GHz, and 22.5 GHz. The radiation pattern for the three-pronged antenna at a representative frequency of 5.5 GHz is shown in Figs. 5(c) and 5(d). The cross-polarization of this antenna is very poor, as shown. The worst-case broadside cross-polarization, which occurs at  $\phi = 326^\circ$ , is only 5.6 dB below the co-polarized power. Also, the radiation is notably asymmetric with respect to  $\phi$ , with maxima at approximately  $\phi = 0^\circ$ ,  $\phi = 120^\circ$ , and  $\phi = 240^\circ$ , corresponding to the angles of the three prongs. The

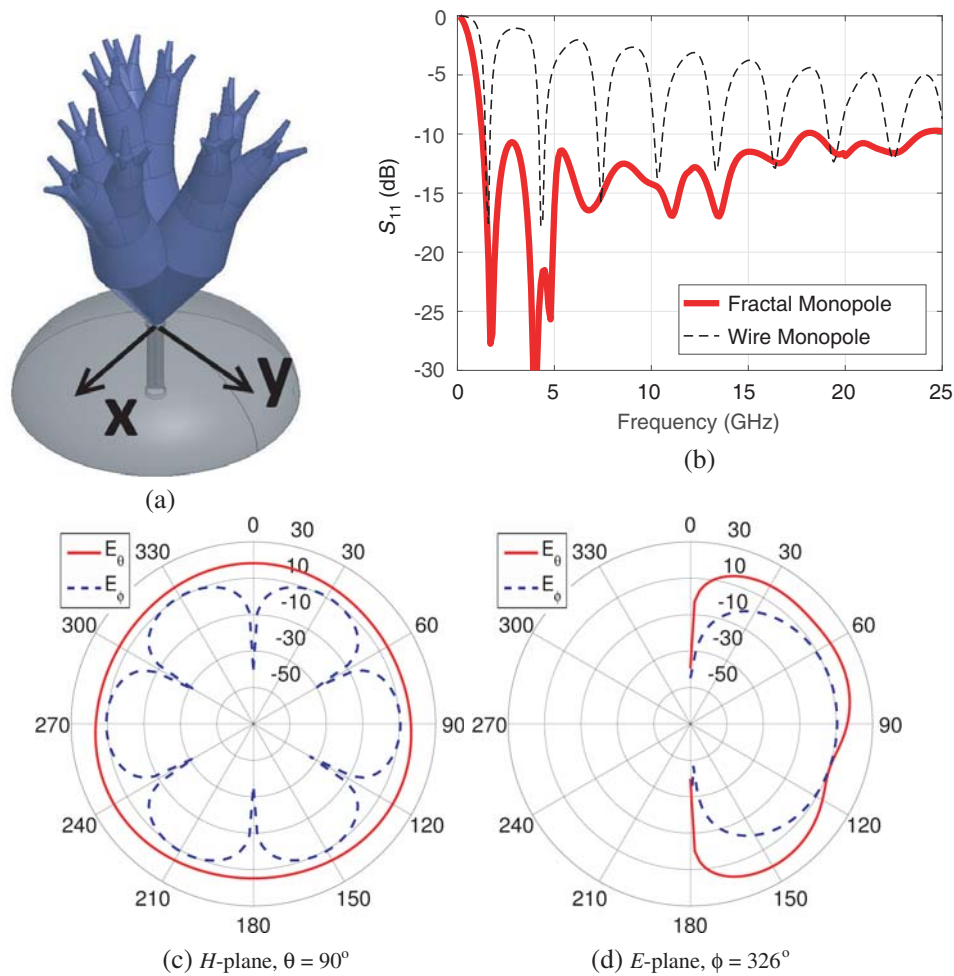


**Figure 5.** (a) A three-pronged, three-iteration fractal tree monopole antenna. (b) The corresponding return loss. (c) The corresponding broadside  $H$ -plane radiation pattern at 5.5 GHz. (d) The corresponding worst-case  $E$ -plane radiation pattern at 5.5 GHz.

radiation minima occur at approximately  $\phi = 60^\circ$ ,  $\phi = 180^\circ$ , and  $\phi = 300^\circ$ , corresponding to the angles of the valleys between the prongs. It is also interesting to note that the cross-polarization has six lobes, with the minima at  $\phi = 0^\circ$  and at  $60^\circ$  intervals all the way around, corresponding to both the prongs and valleys.

The four-pronged fractal antenna shown in Fig. 6(a), which converged with 153,518 tetrahedra, has better bandwidth than the three-pronged version;  $S_{11}$  is shown in Fig. 6(b) to be below  $-10$  dB from approximately 1.23 GHz to 24 GHz, corresponding to a bandwidth of 180.5%. Local minima may be observed in this plot at 1.7 GHz, 4.1 GHz, 4.7 GHz, 6.8 GHz, 11.2 GHz, 13.7 GHz, 16.6 GHz, 20 GHz, and 22.7 GHz. The radiation pattern here, shown in Figs. 6(c) and 6(d), is smoother with respect to  $\phi$  than the three-iteration version, and the broadside cross-polarization is improved to 15.7 dB below the co-polarized power. Again, the radiation pattern is noticeably asymmetric, with minima at  $\phi = 0^\circ$ ,  $\phi = 90^\circ$ ,  $\phi = 180^\circ$ , and  $\phi = 270^\circ$ , at the angles of the prongs, and maxima at  $\phi = 45^\circ$ ,  $\phi = 135^\circ$ ,  $\phi = 225^\circ$ , and  $\phi = 315^\circ$ , at the angles of the valleys. The cross-polarization has eight distinct lobes, with minima at  $\phi = 0^\circ$  and at  $45^\circ$  intervals all the way around, corresponding to both the prongs and the valleys.

Finally, the six-pronged fractal shown in Fig. 7(a) was simulated, and converged with 332,737 tetrahedra. This modification resulted in a lower bandwidth than the five-pronged fractal. Its  $S_{11}$ , shown in Fig. 7(b), is below  $-10$  dB only from 1.2 GHz to 17.9 GHz, corresponding to a bandwidth of 174.9%.

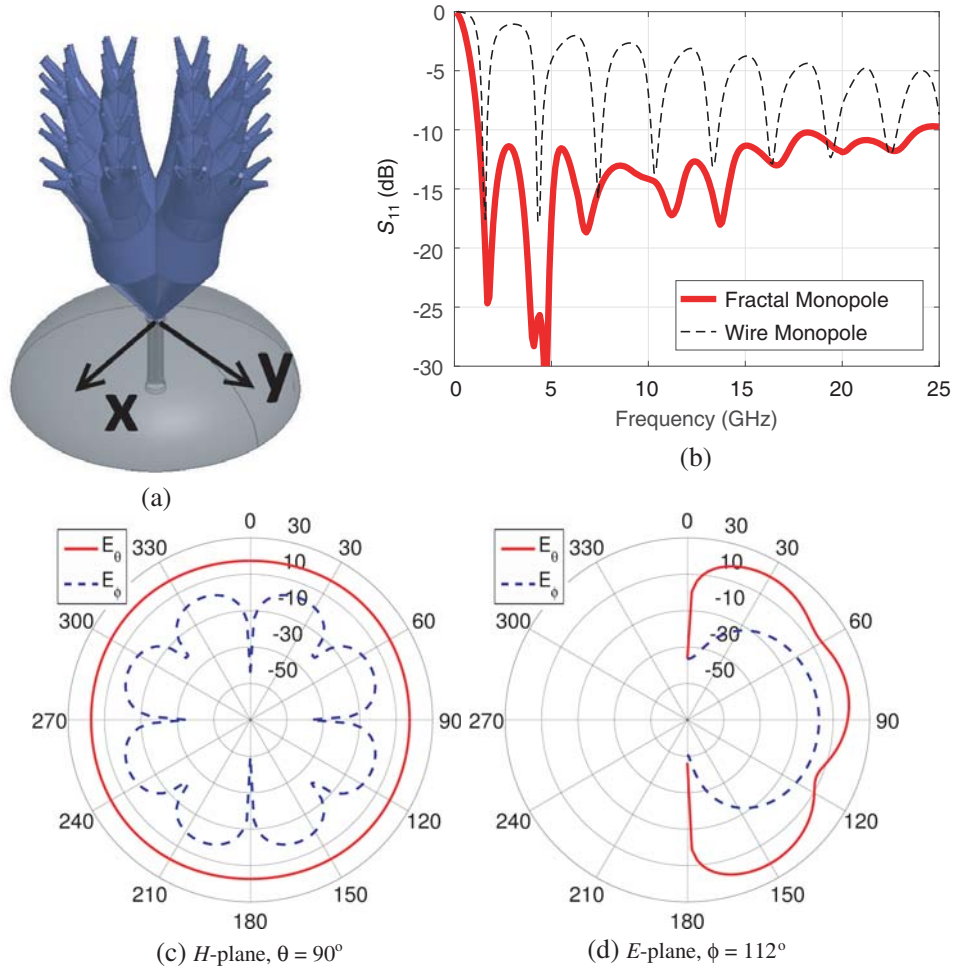


**Figure 6.** (a) A four-pronged, three-iteration fractal tree monopole antenna. (b) The corresponding return loss. (c) The corresponding broadside  $H$ -plane radiation pattern at 5.5 GHz. (d) The corresponding worst-case  $E$ -plane radiation pattern at 5.5 GHz.

**Table 3.** Summary of simulation results for three-pronged, four-pronged, five-pronged, and six-pronged fractal tree monopole antennas at 5.5 GHz.

# of Prongs	Height (mm)	Radius (mm)	Bandwidth (%)	Broadside Cross-pol (dB)	# of Tetrahedra
3	51	27	173.0	5.6	128,303
4	51	27	180.5	15.7	153,518
5	51	27	180.7	27.0	210,702
6	51	27	174.9	42.1	332,737

The radiation pattern for the six-pronged antenna at 5.5 GHz is shown in Figs. 7(c) and 7(d). This antenna has the best polarization of all the prong-number variations, with broadside cross-polarization better than 42.1 dB. The radiation is highly symmetric with respect to  $\phi$ , and the cross-polarization has twelve lobes, with minima at  $\phi = 0^\circ$  and at  $30^\circ$  intervals, corresponding to the prongs and valleys.

Table 3 summarizes the simulation results for the three-pronged, four-pronged, five-pronged, and six-pronged three-iteration fractal tree antennas. As shown, the transition from three prongs to four

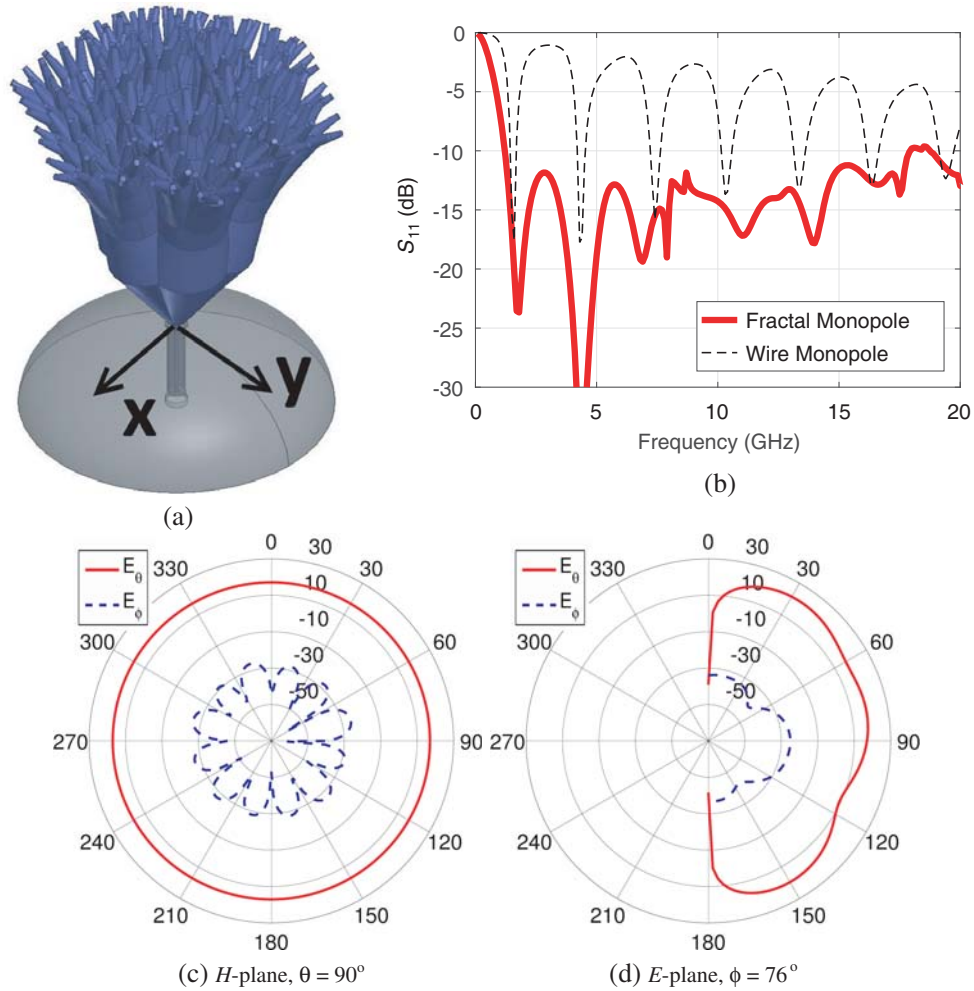


**Figure 7.** (a) A six-pronged, three-iteration fractal tree monopole antenna. (b) The corresponding return loss. (c) The corresponding broadside  $H$ -plane radiation pattern at 5.5 GHz. (d) The corresponding worst-case  $E$ -plane radiation pattern at 5.5 GHz.

prongs resulted in a 7.5% increase in bandwidth, and a 10.1 dB improvement in cross-polarization. The transition from four prongs to five prongs provided only a 0.2% increase in bandwidth, but a 11.3 dB improvement in cross-polarization. Finally, the transition from five prongs to six prongs resulted in a decrease of 5.8% in bandwidth, but an improvement of 15.1 dB in cross-polarization.

Since the five-pronged fractal has the best bandwidth and the second-best polarization of these four simulated antennas, it was selected for further investigation. The HFSS mesh operation and air box dimensions were adjusted to allow acquisition of far field results valid from 1 GHz to 20 GHz. Fig. 8 shows the broadside  $H$ -plane and worst-case  $E$ -plane radiation patterns of the five-pronged, three-iteration fractal tree monopole antenna at 1.3 GHz, 10 GHz, 15 GHz, and 20 GHz. These graphs demonstrate a deterioration in polarization characteristics with increased frequency. The worst-case broadside cross-polarization at 1.3 GHz is better than 68 dB below the co-polarized power. The worst-case broadside cross-polarization at 10 GHz is 26 dB. This degrades to 24 dB at 15 GHz, and 16 dB at 20 GHz.

Figure 9 shows the magnitude of the surface currents on the antenna at 1.3 GHz, 5.5 GHz, 15 GHz, and 20 GHz. The range from blue to red is 0 A/m–3 A/m in every case. As shown, the center of the branching top of the fractal structure does not carry much current at any of the four investigated frequencies. Fig. 9(a) shows the currents at 1.3 GHz, where the current is almost entirely on the outside surface of the structure, with some current on the upper branches of the tree at approximately 1 A/m. High-density current reaches halfway up the arms of the fractal, as it does in none of the other three

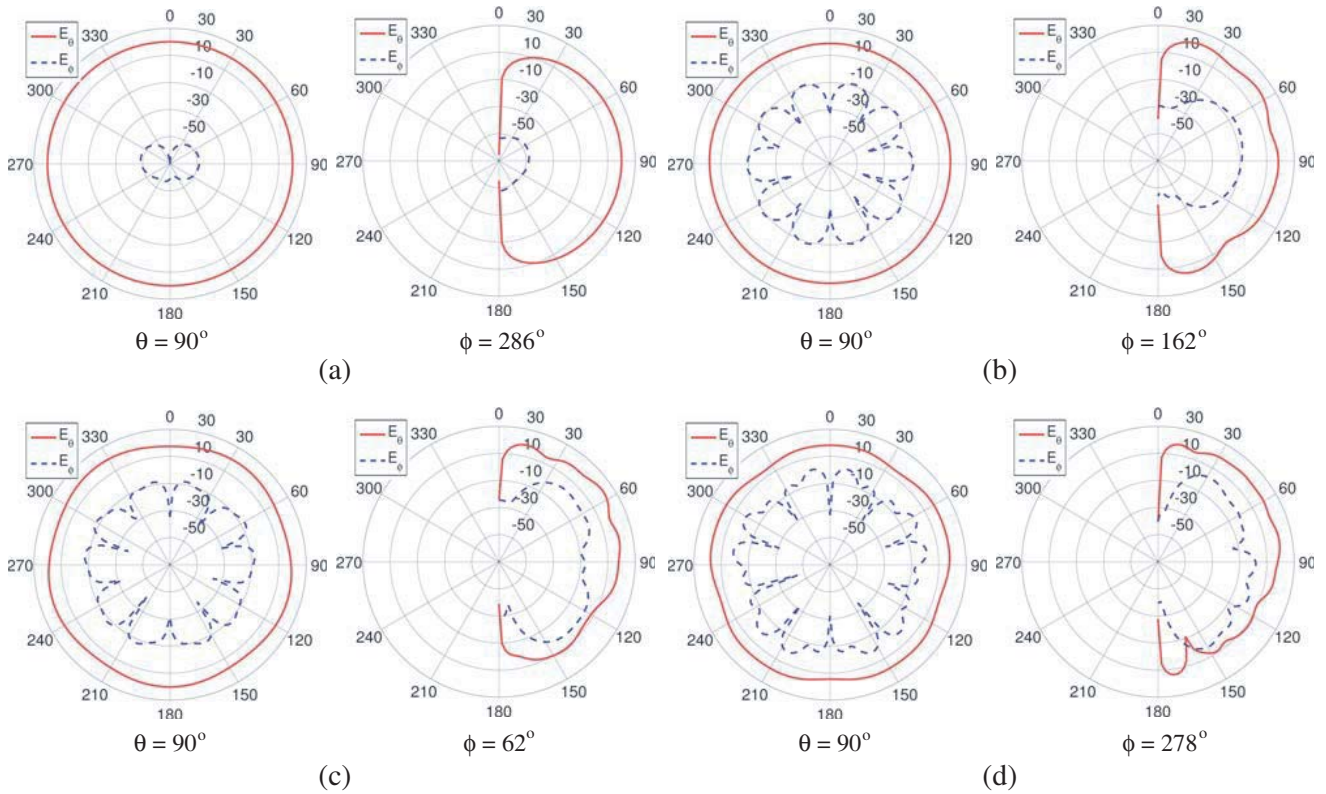


**Figure 8.** Radiation pattern broadside  $H$ -plane and worst-case  $E$ -plane radiation patterns for the five-pronged three-iteration fractal tree antenna at (a) 1.3 GHz, (b) 10 GHz, (c) 15 GHz, and (d) 20 GHz.

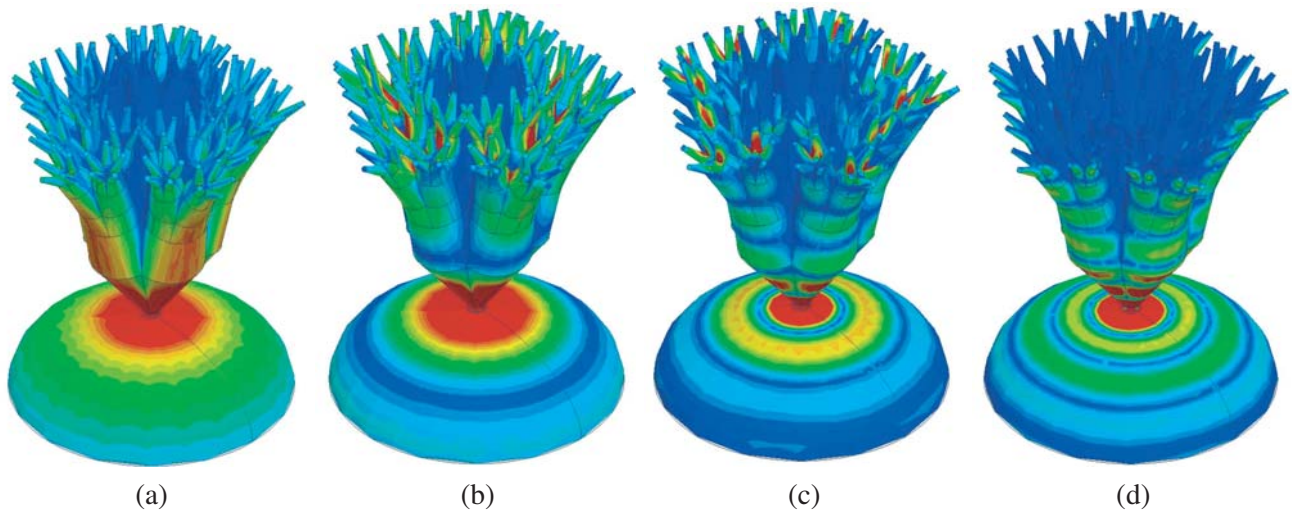


**Figure 9.** Surface currents on the antenna at (a) 1.3 GHz, (b) 5.5 GHz, (c) 15 GHz, and (d) 20 GHz.

figures. Fig. 9(b) shows the currents at 5.5 GHz, where higher current densities are seen in the upper branches of the fractal tree, reaching 3 A/m in the valleys between the second-iteration branches. The high current densities in the upper branches are also visible in Fig. 9(c), at 15 GHz, but in this case they are located in the valleys between the third-iteration branches. Fig. 9(d), shows that the currents at 20 GHz are concentrated most highly at the base of the figure, on the lower half of the first iteration. It should be noted that, though the current distribution is different at each of these frequencies, every

iteration of the fractal structure is actively supporting current across the presented spectrum. As has been seen previously in two-dimensional fractal antennas (see [2]), the large portions of the structure, which would typically be seen as low-frequency features, continue to be active at the higher frequencies of operation. In [2], it was shown that the effect of these features is to capacitively load the antenna and shift the “high frequency” resonances downward.

#### 4. FABRICATION AND MEASUREMENT OF CONICAL FRACTAL TREE MONOPOLE ANTENNA

The Makerbot Replicator 2X 3D printer requires any model it prints to have a qualitatively large base, otherwise the print will not adhere properly to the build plate. It also requires that the model only have minimal spreading with each progressive vertical layer, or the print will become stringy and ill-defined. To facilitate high-quality printing, therefore, the body of the fractal tree was split into two pieces. The upper half of the fractal was printed from bottom to top, and the lower half was printed from top to bottom. The ground was naturally large at the base, and tapered with each layer, so it was not adjusted in any way for the print. Fig. 10(a) shows the HFSS model used for printing. Since the 3D printer requires Stereo Lithography (.stl) files, and HFSS cannot output this file type, a Standard for the Exchange of Product Data (.step) file was exported from HFSS, imported into AutoCad, and exported from AutoCad as a Stereo Lithography file. This was then loaded into the 3D printer Makerware software. The fractal tree and oblate hemispheroidal ground were then 3D printed of ABS plastic with a MakerBot Replicator 2X, using a layer height of 0.1 mm. The bottom and top halves of the fractal body were glued together with superglue. The resulting seam between the top and bottom halves of the fractal body was smoothed using acetone, and the form was spray painted with several layers of an acrylic-based conductive paint from M. G. Chemicals. The conductivity of this spray paint was measured at  $0.6 \Omega/\text{square}$  for a thoroughly coated square. The paint-covered form was then connected to an RG-58C/U coaxial cable using a modified SMA connector embedded in the ground piece of the antenna. This completed antenna is shown in Fig. 10(b). The return loss of this antenna was measured using an Anritsu 37297D network analyzer, and is shown in Fig. 10(c). The corresponding simulated return loss for the five-pronged, three-iteration fractal tree is also shown, for comparison. This antenna was shown to have less than  $-10$  dB return loss over a range of 1.2 GHz–25 GHz, which is a bandwidth of 181.7%.

The printing process resulted in surface roughness that could not be duplicated in simulation, which can be seen especially in the fine details at the top of the fractal tree. Furthermore, the gap between the fractal and the ground, which was set at 0.8 mm in the simulations, was much harder to fix in reality, and may have varied from the target value by as much as a millimeter or two. Also, because the fractal

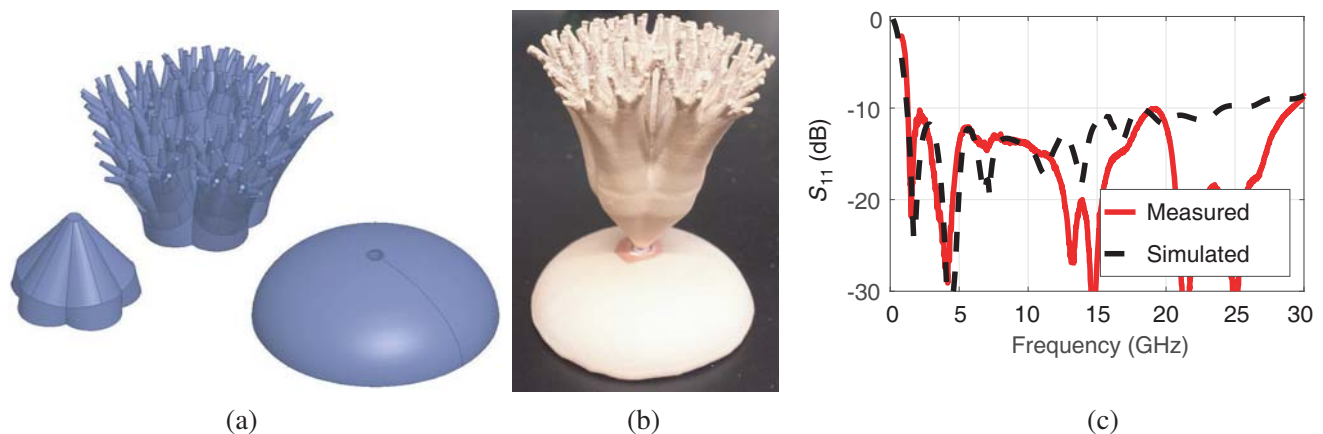


**Figure 10.** (a) 3D printed pieces of fractal monopole antenna. (b) Final fractal tree antenna, with conductive spray-paint coating. (c) Measured (solid red) and simulated (dashed black) return loss in dB.

body was printed in two pieces, there was a noticeable seam around the circumference of the body, as shown in Fig. 10(b). Finally, in simulation the antenna body and ground were defined as PEC, but in reality they had a finite conductivity that almost certainly varied over the surface, since some areas were extremely difficult to access with the spray paint. Any or all of these variations may have contributed to the difference between simulated and measured results shown in Fig. 10(c).

## 5. CONCLUSION

A fractal tree monopole antenna with a cone-and-connector basic repeating form is presented. The number of fractal iterations and number of prongs were optimized through simulation of one-iteration, two-iteration, three-iteration, three-prong, four-prong, five-prong, and six-prong models. The three-iteration, five-prong model was found to have the best bandwidth performance at 180% percent bandwidth. This model also showed more than 27 dB of differentiation between the broadside copolarization and cross-polarization. This antenna was fabricated using 3D printing techniques and coated with a conductive spray paint. Measurement of the antenna return loss confirmed an operative bandwidth of more than 180%.

## REFERENCES

1. Bandelbrot, B. B., *The Fractal Geometry of Nature*, Macmillan, 1983.
2. Puente-Baliarda, C., J. Romeu, R. Pous, and A. Cardama, "On the behavior of the Sierpinski multiband fractal antenna," *IEEE Trans. Antennas Propag.*, Vol. 46, No. 4, 517–524, 1998.
3. Naser-Moghadas, M., R. A. Sadeghzadeh, T. Aribi, T. Sedghi, and B. S. Virdee, "UWB monopole microstrip antenna using fractal tree unit-cells," *Microw. Opt. Technol. Lett.*, Vol. 54, No. 10, 2366–2370, 2012.
4. Pourahmadazar, J., C. Ghobadi, and J. Nourinia, "Novel modified pythagorean tree fractal monopole antennas for UWB applications," *IEEE Antennas Wirel. Propag. Lett.*, Vol. 10, 484–487, 2011.
5. Mahatthanajatuphat, C., P. Akkaraekthalin, S. Saleekaw, and M. Krairiksh, "Bidirectional multiband antenna with modified fractal slot fed by CPW," *Progress In Electromagnetics Research*, Vol. 95, 59–72, 2009.
6. Mahatthanajatuphat, C., S. Saleekaw, P. Akkaraekthalin, and M. Krairiksh, "A Rhombic patch monopole antenna with modified Minkowski fractal geometry for UMTS, WLAN, and mobile WiMAX application," *Progress In Electromagnetics Research*, Vol. 89, 57–74, 2009.
7. Hamdy, S., A. El-Khouly, A. Zaki, and S. E. El-Khamy, "A new fractal-like tree structure of circular patch antennas for 5G multi-band and wide-band applications," *2016 Progress In Electromagnetics Research Symposium (PIERS)*, 2467–2467, Shanghai, China, August 8–11, 2016.
8. Petko, J. S. and D. H. Werner, "Miniature reconfigurable three-dimensional fractal tree antennas," *IEEE Trans. Antennas Propag.*, Vol. 52, No. 8, 1945–1956, 2004.
9. Rmili, H., O. El Mrabet, J. Floc'h, and J. Miane, "Study of an electrochemically-deposited 3-D random fractal tree-monopole antenna," *IEEE Trans. Antennas Propag.*, Vol. 55, No. 4, 1045–1050, 2007.
10. Smith, K. L. and R. S. Adams, "A novel ultra-wideband fractal monopole antenna," *IEEE Int. Symp. on Ant. and Prop. (APSURSI)*, 2315–2316, 2015.